# Title: Distinct place cell dynamics in CA1 and CA3 encode experience in new contexts

**Authors:** Can Dong[1] and Mark E. J. Sheffield[1*]

**Affiliations:**

[1] Department of Neurobiology and Grossman Institute for Neuroscience, Quantitative Biology and Human Behavior, University of Chicago, Chicago, IL 60637, USA.

[*] Correspondence to: sheffield@uchicago.edu.

**Abstract:** We compared trial-by-trial dynamics of place cells in CA1 and CA3 in new contexts across days. We found that CA1 place fields form early but shift backwards with experience and partially remap across days. In contrast, CA3 place fields develop gradually but remain stable with experience and across days. This suggests distinct plasticity mechanisms drive the formation and dynamics of place fields in CA1 and CA3 to encode distinct features of experience.

**Main text:** The hippocampus plays a critical role in learning by rapidly forming and continuously updating experience-driven representations in the brain[1,2]. Representations of contextual experience are encoded and recalled by populations of place cells in hippocampal sub-regions CA1, CA3, and dentate gyrus[3,4]. Synaptic plasticity within these sub-regions is the key process that alters and stores representations and comes in many forms[5,6]. Understanding how place cell representations form, evolve, and are recalled within distinct hippocampal sub-regions during novel experiences can therefore provide key insights into the types of synaptic plasticity mechanisms that are at play during learning and memory recall. Further, because synaptic plasticity mechanisms can work on rapid timescales to continually alter place cell activity, it is essential to determine the real-time place cell dynamics on a trial-by-trial basis. However, the trial-by-trial dynamics of hippocampal place cells during the first moments of a novel experience and throughout ongoing experience measured over long timescales (across days) has not been systematically compared between CA1 and CA3.

To address this, we expressed GCaMP6f in either the CA1 or CA3 sub-region of different mice (Fig. 1c, d). The Grik4-cre line[7] was used to restrict expression to CA3 pyramidal neurons (Fig.

1c). Using 2-photon microscopy we then recorded calcium transients from pyramidal cell populations in both regions (Extended Data Fig. 1)[8,9]. On experimental day 1 mice were exposed to a familiar (F) context before being switched to a novel context (N1) (Fig. 1a)[9]. On experimental day 2, mice experienced the same F-to-N switch but to a different N context (N2; Fig. 1a). N1 and N2 were grouped together and are referred to as N. Mice momentarily slowed down after the transition between contexts (Fig. 1b), confirming their perception of the switch. This paradigm led to many repeated traversals in both contexts with matched behavior, allowing lap-by-lap place field (PF) dynamics to be measured systematically and compared across F and N contexts without confounds caused by changes in behavior.

Upon exposure to N, both CA1 and CA3 place cells globally remapped (Fig. 1e, f) and displayed altered PFs compared to F (Extended Data Fig. 2). Crucially, we wanted to observe the real-time formation of new place cells in CA1 and CA3 to examine potential differences in their formation dynamics. Therefore, formation of new PFs in N was quantified on a lap-by-lap basis (Fig. 1g-i). Some PFs formed instantly, i.e. on the first lap (Instant PFs; Fig. 1g; left), while others were delayed by several laps (Delayed PFs; Fig. 1g; right). Similar to previous observations, many CA1 PFs formed rapidly[6,9], with a high proportion of instant PFs (30%; Fig. 1h, i). Unexpectedly, only 9% of CA3 PFs were instant and the distribution of PF onset laps was more uniform, indicating CA3 place cell representations form more gradually than CA1 representations (Fig. 1h, i; Extended Data Fig. 2c, d). Supporting this, CA1 place cell activity decoded position on the first lap better than CA3 place cell activity (Fig. 1j-l, Extended Data Fig. 3). These data suggest that in a novel context, CA1 instantly forms a well-organized map, whereas CA3 forms a map gradually with experience.

What do these observations suggest about synaptic plasticity mechanisms? First, some models of CA1 place field formation require the presence of spatially tuned presynaptic inputs from CA3[5,10]. In this scheme, spatially tuned CA3 inputs coincident with inputs from entorhinal cortex (EC) generate dendritic plateau potentials in CA1 cells that drive synaptic potentiation[11]. The lack of spatially tuned CA3 cells that we found on lap 1 suggests CA1 instant place fields are not formed through this mechanism, and may instead form through other direct inputs from EC or Nucleus Reunions [12]. Second, delayed CA1 PFs have been proposed to form through a process of local dendritic spikes that occur on the initial laps in the absence of somatic firing. This potentiates local clusters of synapses that become strong enough to drive firing, and possibly plateau potentials, after a delay, to form new PFs[6,9-11,13,14]. Because we found the vast majority of CA3 PFs form after a delay, our data suggest a similar mechanism is at play in CA3.

To examine plasticity mechanisms occurring after PFs have formed in CA1 and CA3, we tracked new PFs throughout experience in N. We compared the first and second half of N and found CA3 PFs were more stable than CA1 PFs (Fig. 2a). Next, we computed each PF's center of mass (COM) on a lap-by-lap basis in N in both regions. Some PFs were stable throughout N, whereas others shifted systematically throughout the session (Fig. 2b). Averaging across the PF population, PFs shifted backwards in both regions, but significantly more so in CA1 than CA3 (Fig. 2c, Extended Data Fig. 4).

Asymmetric synaptic plasticity mechanisms, such as spike-timing-dependent plasticity (STDP)[15] and behavioral time-scale plasticity (BTSP)[5,10], predict such backward shifting[15]. These two forms of plasticity occur over different timescales (milliseconds for STDP, seconds for BTSP), so

we calculated the timescale of backward shifting CA1 PFs to determine which form of plasticity may be occurring. Based on the ability of STDP to potentiate synapses activated up to ~20 ms prior to postsynaptic firing[16], we calculated PFs would shift maximally 0.48 ± 0.15 cm/lap (mean ± SD) through STDP based on the average running speed of our mice (24.1 ± 7.5 cm/s mean ± SD). On average, backward shifting PFs in CA1 shifted by 0.34 ± 0.34 cm/lap (mean ± SD). This provides strong support that STDP is the mechanism driving continuous backward shifting. Further, STDP is known to occur at CA1-CA3 synapses[16] and given the relative stability of CA3 PFs concurrent with the CA1 backward shifting PFs we observed here, it suggests STDP is occurring at these synapses to drive the backward shifting of CA1 PFs (although other synapses could also be involved).

Memory recall of spatial contexts is supported by the reactivation of stable PFs upon re-exposures[4]. We therefore examined the same place cells upon re-exposure to N across days (Fig. 3a). On day 2, mouse behavior on the first lap of N revealed mice had become more familiar with N (Extended Data Fig. 5a, b). We then quantified the spatial correlation of mean PFs identified on N day 1 with N day 2 (Fig. 3b-e), which was on average significantly higher in CA3 than CA1 (Fig. 3c-e). The bimodal distribution of CA3 PF spatial correlations (Fig. 3c; bottom), helped categorize PFs as either stable (spatial correlation > 0.5, green) or unstable (< 0.5; light-green). In all mice we found that CA3 had a higher fraction of stable PFs compared to CA1 in (Fig. 3d).

We then compared the PF onset laps of stable PFs on day 2 (Fig. 3f, left) with PFs that newly formed on day 2, which included both unstable PFs from day 1 (Fig. 3f, middle) and PFs that

92 appeared for the first time on day 2 (Fig. 3f, right). We found that stable PFs appeared earlier in
93 the session than newly formed PFs, and this difference was much more significant in CA3 than
94 CA1 (Fig. 3g). This also shows that a high proportion of CA1 PFs are continuously forming even
95 as the context becomes familiar. These findings reveal that place cell representations that form
96 following exposure to novel contexts are more stable in CA3 than CA1. Stable PFs are instantly
97 reactivated on the second day of exposure and the CA1 continuously forms a high proportion of
98 new PFs. The greater reorganization of CA1 place cell representations across exposures
99 suggests offline plasticity in the CA1, possibly occurring during sleep[17].

100 Is the reorganization of CA1 PFs across days due to a continuation of the backward shifting that
101 occurs within the session on day 1, possibly during offline activation, or a process more akin to
102 partial/global remapping? To answer this, we calculated the difference between each PF's COM
103 on the last active lap on day 1 and first active lap in day 2 (Fig. 3h). The mean of the
104 distributions in both CA1 and CA3 were not statistically different from 0 (Fig. 3h), revealing no
105 evidence for systematic backward shifting occurring offline. This shows that backward shifting is
106 an experience-dependent process and the reorganization of CA1 PFs across days is a process
107 akin to partial/global remapping.

108 Lastly, we determined whether the backward shifting we had observed on day 1 in N continued
109 upon re-exposure to N on day 2. We found that lap-by-lap the CA1 systemically shifted
110 backwards throughout the first part of the session, yet the CA3 map remained relatively stable
111 throughout the session (Fig. 3i). This was also true in F (Extended Data Fig. 6), although the
112 extent of CA1 backward shifting decreased with familiarity. This shows that asymmetric CA1

plasticity mechanisms are occurring in novel and familiar contexts, but the level of novelty enhances this process.

What might be the function of these differences in the formation and plasticity of place cell representations in CA1 and CA3? First, instant CA1 PFs could mediate the ability of the hippocampus to rapidly learn and store episodes of events on a single trial[18]. The backward shifting of the PF population we observed during ongoing experience could allow the CA1 to gradually predict future locations within a context[5,19]. Indeed, asymmetric plasticity rules automatically produce predictions of the future by strengthening synapses that are activated earlier along the track with each traversal[15]. The CA1, then, rapidly generates unique representations of the world that are then continuously shaped by exploratory experience to predict the near future (where am I going?). In parallel, the CA3 gradually forms representations that are preserved during experience and encode the present moment (where am I currently?). This function seemingly extends across time as relatively stable CA3 place cell representations are rapidly reinstated upon re-exposure to the same context, possibly to support memory recall. Offline reorganization of CA1 place cell representations across days may instead serve to separate events occurring in the same context into distinct memories[20]. This framework is depicted in a conceptual model in Extended Data Fig. 7. Given the known circuitry between CA3 and CA1, the independent nature of CA1 encoding relative to CA3 (instant PF formation and reorganization across days) suggests the formation and recall of CA1 place cell representations is substantially influenced by other inputs (Entorhinal cortex and Nucleus Reunions[12]).

**Acknowledgments:** We thank D. Dombeck and A. Madar for comments on the manuscript, C. Cherian for helpful manuscript edits, and members of Sheffield lab for manuscript comments and useful discussions. **Funding:** This work was supported by: The Whitehall Foundation, The Searle Scholars Program, The Sloan Foundation, The University of Chicago Grossman Institute for Neuroscience start-up funds, and the NIH (1DP2NS111657-01). **Author contributions:** C.D. performed surgeries, collected the data, wrote the analysis code and analyzed data. M.S. and C.D. conceived and designed the experiments and interpreted the data. M.S. wrote the manuscript with feedback from C.D. **Competing interests:** Authors declare no competing interests and **Data and materials availability:** Scripts used for data analysis are available on Github and raw data is available upon request.

**References:**

1 Parisi, G. I., Kemker, R., Part, J. L., Kanan, C. & Wermter, S. Continual lifelong learning with neural networks: A review. *Neural Netw* **113**, 54-71, doi:10.1016/j.neunet.2019.01.012 (2019).

2 Kitamura, T. *et al.* Engrams and circuits crucial for systems consolidation of a memory. *Science* **356**, 73-78, doi:10.1126/science.aam6808 (2017).

3 Hainmueller, T. & Bartos, M. Parallel emergence of stable and dynamic memory engrams in the hippocampus. *Nature* **558**, 292-296, doi:10.1038/s41586-018-0191-2 (2018).

4 Dupret, D., O'Neill, J., Pleydell-Bouverie, B. & Csicsvari, J. The reorganization and reactivation of hippocampal maps predict spatial memory performance. *Nat Neurosci* **13**, 995-1002, doi:10.1038/nn.2599 (2010).

5 Magee, J. C. & Grienberger, C. Synaptic Plasticity Forms and Functions. *Annu Rev Neurosci*, doi:10.1146/annurev-neuro-090919-022842 (2020).

6 Sheffield, M. E. & Dombeck, D. A. Dendritic mechanisms of hippocampal place field formation. *Curr Opin Neurobiol* **54**, 1-11, doi:10.1016/j.conb.2018.07.004 (2019).

7 Nakazawa, K. *et al.* Requirement for hippocampal CA3 NMDA receptors in associative memory recall. *Science* **297**, 211-218, doi:10.1126/science.1071795 (2002).

8 Sheffield, M. E. & Dombeck, D. A. Calcium transient prevalence across the dendritic arbour predicts place field properties. *Nature* **517**, 200-204, doi:10.1038/nature13871 (2015).

9 Sheffield, M. E. J., Adoff, M. D. & Dombeck, D. A. Increased Prevalence of Calcium Transients across the Dendritic Arbor during Place Field Formation. *Neuron* **96**, 490-504 e495, doi:10.1016/j.neuron.2017.09.029 (2017).

10 Bittner, K. C., Milstein, A. D., Grienberger, C., Romani, S. & Magee, J. C. Behavioral time scale synaptic plasticity underlies CA1 place fields. *Science* **357**, 1033-1036, doi:10.1126/science.aan3846 (2017).

11 Bittner, K. C. *et al.* Conjunctive input processing drives feature selectivity in hippocampal CA1 neurons. *Nat Neurosci* **18**, 1133-1142, doi:10.1038/nn.4062 (2015).

12 Dolleman-van der Weel, M. J. *et al.* The nucleus reuniens of the thalamus sits at the nexus of a hippocampus and medial prefrontal cortex circuit enabling memory and behavior. *Learn Mem* **26**, 191-205, doi:10.1101/lm.048389.118 (2019).

13 Cohen, J. D., Bolstad, M. & Lee, A. K. Experience-dependent shaping of hippocampal CA1 intracellular activity in novel and familiar environments. *Elife* **6**, doi:10.7554/eLife.23040 (2017).

14 Diamantaki, M. *et al.* Manipulating Hippocampal Place Cell Activity by Single-Cell Stimulation in Freely Moving Mice. *Cell Rep* **23**, 32-38, doi:10.1016/j.celrep.2018.03.031 (2018).

15 Mehta, M. R., Quirk, M. C. & Wilson, M. A. Experience-dependent asymmetric shape of hippocampal receptive fields. *Neuron* **25**, 707-715, doi:10.1016/s0896-6273(00)81072-7 (2000).

16 Dan, Y. & Poo, M. M. Spike timing-dependent plasticity of neural circuits. *Neuron* **44**, 23-30, doi:10.1016/j.neuron.2004.09.007 (2004).

17 Sadowski, J. H., Jones, M. W. & Mellor, J. R. Sharp-Wave Ripples Orchestrate the Induction of Synaptic Plasticity during Reactivation of Place Cell Firing Patterns in the Hippocampus. *Cell Rep* **14**, 1916-1929, doi:10.1016/j.celrep.2016.01.061 (2016).

18 Lee, S. W., O'Doherty, J. P. & Shimojo, S. Neural computations mediating one-shot learning in the human brain. *PLoS Biol* **13**, e1002137, doi:10.1371/journal.pbio.1002137 (2015).

19 Stachenfeld, K. L., Botvinick, M. M. & Gershman, S. J. The hippocampus as a predictive map. *Nat Neurosci* **20**, 1643-1653, doi:10.1038/nn.4650 (2017).

20 Clewett, D., DuBrow, S. & Davachi, L. Transcending time in the brain: How event memories are constructed from experience. *Hippocampus* **29**, 162-183, doi:10.1002/hipo.23074 (2019).

21 Dombeck, D. A., Harvey, C. D., Tian, L., Looger, L. L. & Tank, D. W. Functional imaging of hippocampal place cells at cellular resolution during virtual navigation. *Nat Neurosci* **13**, 1433-1440, doi:10.1038/nn.2648 (2010).

22 Heys, J. G., Rangarajan, K. V. & Dombeck, D. A. The functional micro-organization of grid cells revealed by cellular-resolution imaging. *Neuron* **84**, 1079-1090, doi:10.1016/j.neuron.2014.10.048 (2014).

23 Aronov, D., Nevers, R. & Tank, D. W. Mapping of a non-spatial dimension by the hippocampal-entorhinal circuit. *Nature* **543**, 719-722, doi:10.1038/nature21692 (2017).

24 Mukamel, E. A., Nimmerjahn, A. & Schnitzer, M. J. Automated analysis of cellular signals from large-scale calcium imaging data. *Neuron* **63**, 747-760, doi:10.1016/j.neuron.2009.08.009 (2009).

25 Tampuu, A., Matiisen, T., Olafsdottir, H. F., Barry, C. & Vicente, R. Efficient neural decoding of self-location with a deep recurrent network. *PLoS Comput Biol* **15**, e1006822, doi:10.1371/journal.pcbi.1006822 (2019).

26 Ho, J., Tumkaya, T., Aryal, S., Choi, H. & Claridge-Chang, A. Moving beyond P values: data analysis with estimation graphics. *Nat Methods* **16**, 565-566, doi:10.1038/s41592-019-0470-3 (2019).

27 Dragoi, G. & Tonegawa, S. Preplay of future place cell sequences by hippocampal cellular assemblies. *Nature* **469**, 397-401, doi:10.1038/nature09633 (2011).

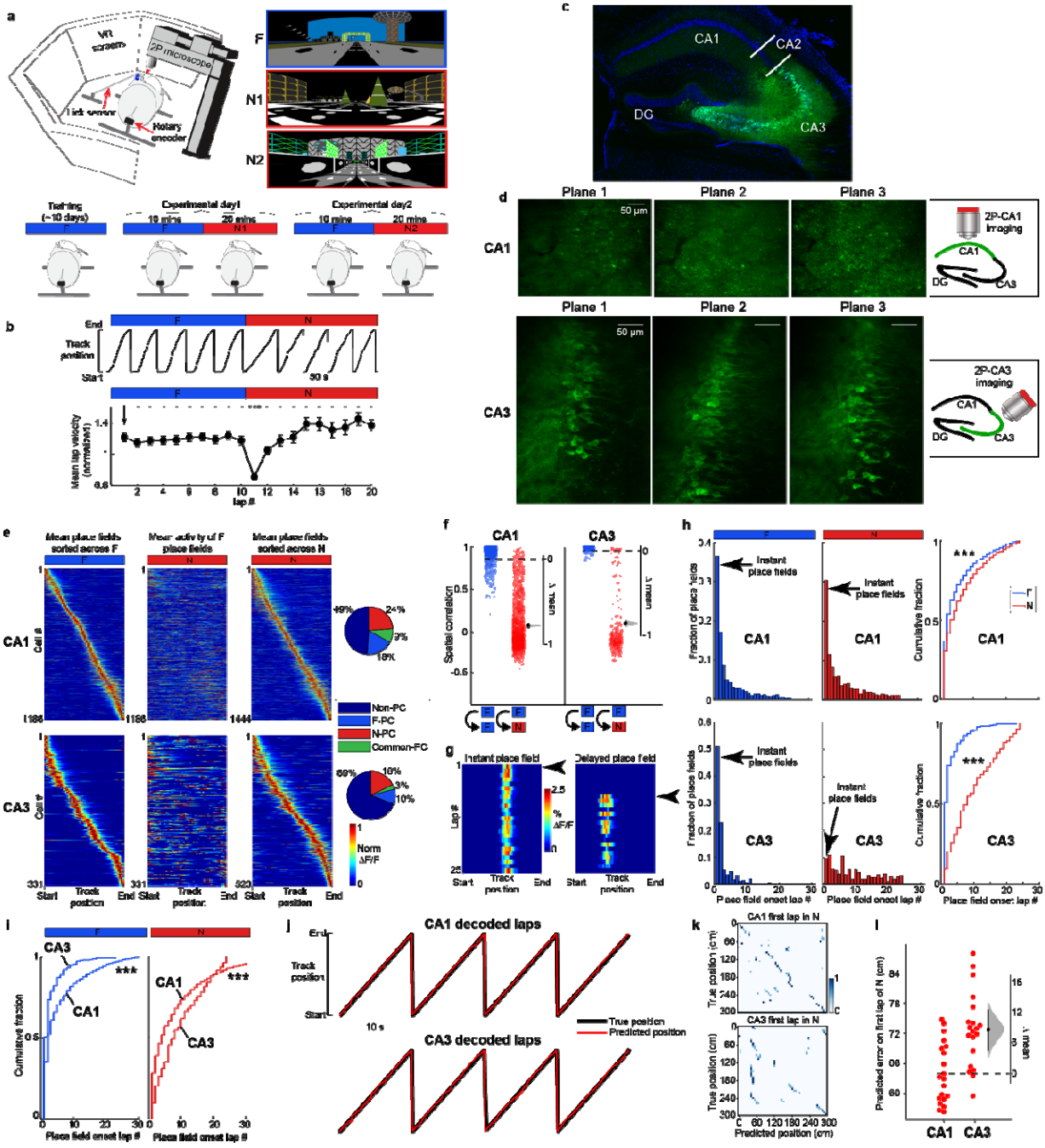


**Fig. 1: Place field formation in novel contexts is rapid in CA1 but gradual in CA3**

**a,** Top left, depiction of the virtual reality (VR) set up. Top right, the familiar (F) and two novel (N1 and N2) contexts. Bottom: Scheme of the experimental procedure. **b,** Top: Single mouse behavior showing track position versus time during an F to N switch. Bottom: Summary data across all mice of mean lap velocity during F and N (*n* = 20 sessions in 11 mice). Lap velocity is

normalized to the mean lap velocity in each mouse ± SEM, and each lap is compared to the first lap in F using a one-way ANOVA with Tukey HSD post hoc test. ***, $P < 0.001$. **c,** Brain slice showing specific CA3 expression of cre-dependent GCaMP6f (green) and DAPI for nuclei (blue) from a Girk4-cre transgenic mouse. **d,** Example field of views (FOV) from multiplane imaging in CA1 (top) and CA3 (bottom). Right: scheme of the position for the objective during imaging. Scale bar = 50 µm. **e,** Left: mean place fields in F sorted by track position. Middle: mean activity of the same neurons on the left in N. Right: mean place fields in N sorted by track position. Far right: Percentage of place cells in F and N or common to both from all active neurons. CA1, top panels; CA3, bottom panels. ΔF/F activity is normalized to each neurons' maximum transient. *n* = 7 sessions in 4 mice for CA1, *n* = 13 sessions in 7 mice for CA3. **f,** Pearson's correlation coefficient of each cell's mean place field within F (blue) and between F and N (red). Estimation plots of mean difference (Δ) shown on the right of each plot (see Methods). **g,** Example of an instant place field (left) and delayed place field (right) in N. Arrows indicate the place field onset lap. **h,** Histograms of place field onset laps in F (left) and N (middle) and cumulative fraction plots for F and N (right). Wilcoxon rank sum test. ***, $P < 0.001$. **i,** Cumulative fraction plots for CA1 and CA3 place field onset lap in F (left) and in N (right). Wilcoxon rank sum test. ***, $P < 0.001$. **j,** Example mouse showing actual track position (black) on laps 37-40 and the predicted position (red) decoded by an LSTM decoder (see Methods). CA1, top; CA3, bottom. **k,** Confusion matrix between the predicted (x-axis) and the real (y-axis) position for the first lap in N. **l,** Predicted error on the first lap in N for CA1 and CA3. Each dot represents the decoding error for one decoder trial built based on the activity of 200 randomly chosen place cells from

244 CA1 (left) or CA3 (right). *n* = 20 decoder trials. Estimation plot of mean difference (Δ) shown on

245 the right.

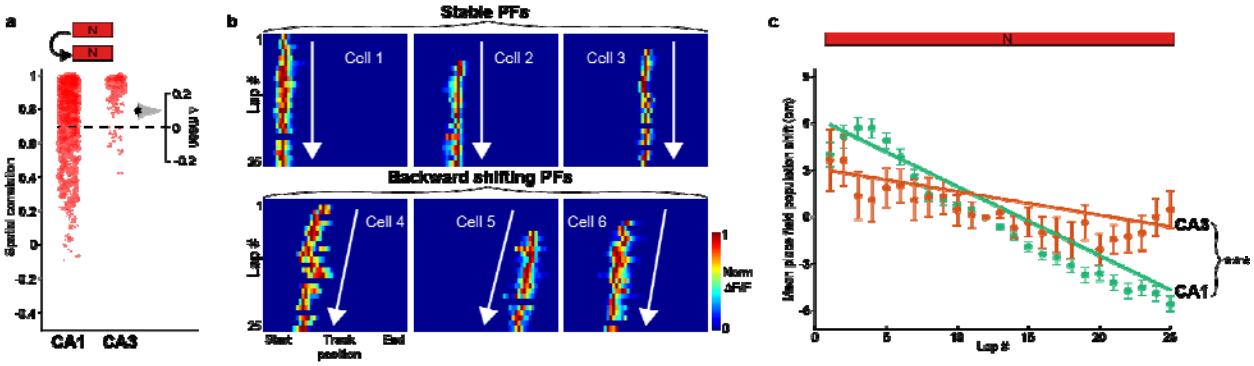


**Fig. 2: CA3 place fields exhibit relative stability while CA1 place fields continuously shift backwards with experience in novel contexts**

**a,** Spatial correlation (Pearson's correlation coefficient) of mean place field activity within N (first half versus second half of session in N). Estimation plot of mean difference (Δ) between CA1 and CA3 shown on the right. **b,** 6 example place cells with stable place fields (top) or backward shifting place fields (bottom) in N. Place field transients shown lap-by-lap for the first 25 laps. White arrows depict the direction of place fields with experience. **c,** Mean ± SEM place field shift from all place cells and all mice lap-by-lap in N in CA1 (green; *n* = 1444 cells from 4 mice;) and CA3 (orange; *n* = 520 cells from 7 mice;). For each place cell the COM of place field transients on each lap was compared to the COM of place field transients on lap 12. Regression lines are depicted on top of data and have statistically different slopes. ***, $P < 0.001$.

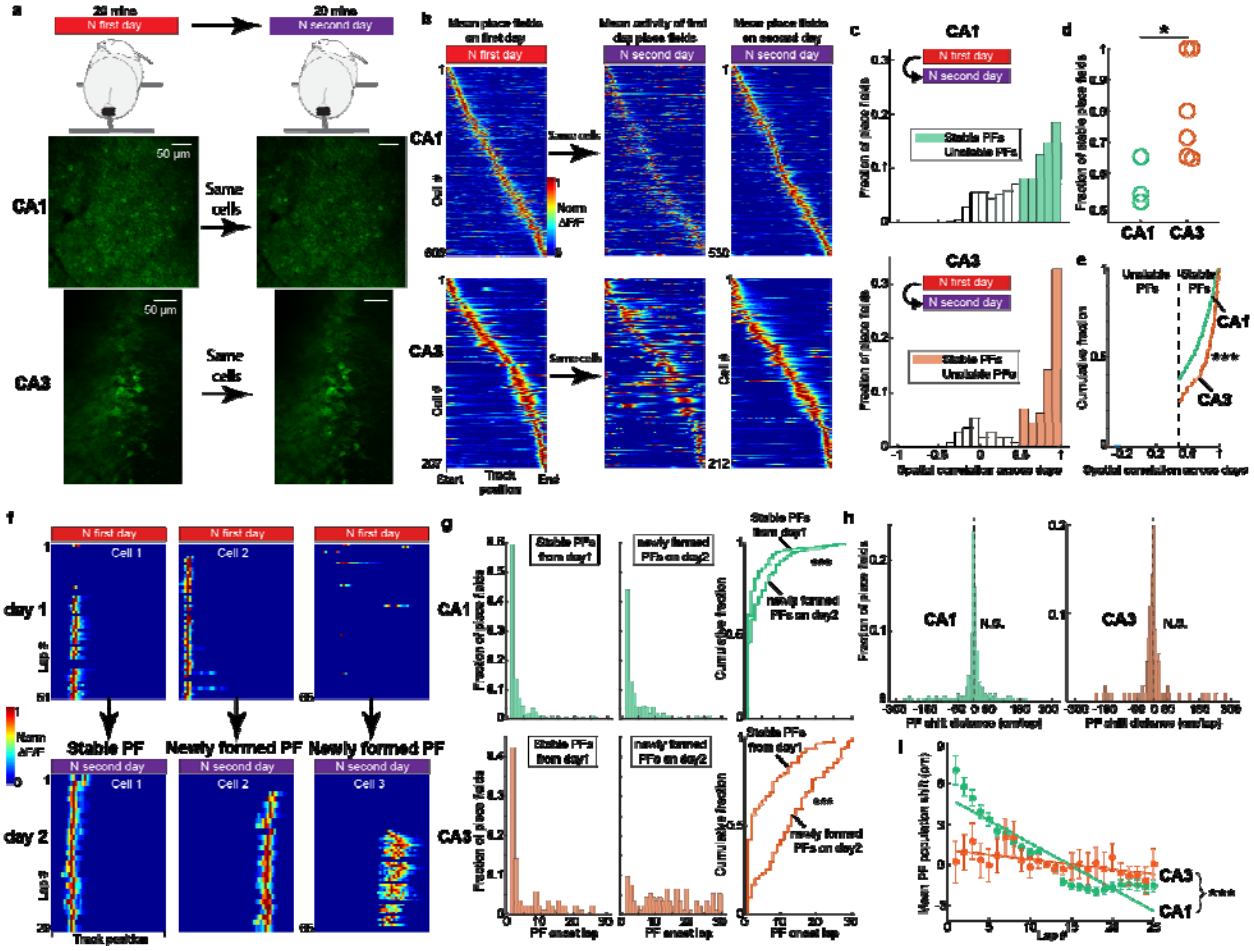


**Fig. 3: CA3 place fields exhibit higher stability across days than CA1 place fields**

**a,** Experimental setup. Top: mice are recorded for 20 min in N across 2 days. Bottom: example field of view from one imaging plane from CA1 and CA3 across 2 days showing the same cells. scale bar = 50 µm. **b,** Left: mean place fields in N on day 1 sorted by track position. Middle: mean activity of the same neurons on the left on day 2 in N. Right: mean place fields in N on day 2 sorted by track position. **c,** Histograms of Pearson's correlation coefficient of mean place field activity across days in N (only place cells with place fields on both days were used). Spatial correlations greater than 0.5 were considered stable place fields and less than 0.5 unstable. **d,** Fraction of stable place fields across days per mouse in CA1 and CA3. Unpaired t-test. *P<0.05.

**e,** Cumulative fraction plots of Pearson's correlation coefficient in N across days in CA1 and CA3 from the same data shown in (**c**). Wilcoxon rank sum test. ***, $P < 0.001$. **f,** Example of a stable place field (left), an unstable place field with a newly formed place field on day 2 (middle) and a newly formed place field on day 2 (right). Place field transients shown lap by lap for all laps in N on day 1 and day 2 from the same 3 cells. **g,** Histograms of place field onset laps in N on day 2 for stable place fields (left), and newly formed place fields (middle) in CA1 (top) and CA3 (bottom). Right: cumulative fraction plots of histogram data. Wilcoxon rank sum test. ***, $P < 0.001$. **h**, Histogram of place field shifts across days for CA1 (left) and CA3 (right). The shifts were calculated by the difference between each place field's COM of the last active lap on day 1 and first active lap in day 2. Only place cells with place fields on both days are included. Wilcoxon signed rank test, N.S., $P > 0.05$. **i,** Mean ± SEM place field shift from all place cells and all mice lap-by-lap in N on day 2 in CA1 (green; $n = 530$ cells from 3 mice) and CA3 (orange; $n = 212$ cells from 6 mice). For each place cell the COM of place field transients on each lap was compared to the COM of place field transients on lap 12. Regression lines are depicted on top of data. ***, $P < 0.001$.